Earth **Surface**
Dynamics

Suitability of ground-based SfM–MVS for monitoring glacial and periglacial processes

Livia Piermattei[1,2], Luca Carturan[2], Fabrizio de Blasi[2], Paolo Tarolli[2], Giancarlo Dalla Fontana[2], Antonio Vettore[3], and Norbert Pfeifer[1]

[1]Department of Geodesy and Geoinformation, TU Wien, Vienna, Austria
[2]Department of Land, Environment, Agriculture and Forestry, University of Padova, Padova, Italy
[3]Interdepartment Research Center of Geomatics, University of Padova, Padova, Italy

Correspondence to: Livia Piermattei (livia.piermattei@studenti.unipd.it)

Abstract. Photo-based surface reconstruction is rapidly emerging as an alternative survey technique to lidar (light detection and ranging) in many fields of geoscience fostered by the recent development of computer vision algorithms such as structure from motion (SfM) and dense image matching such as multi-view stereo (MVS). The objectives of this work are to test the suitability of the ground-based SfM–MVS approach for calculating the geodetic mass balance of a $2.1\,\mathrm{km}^2$ glacier and for detecting the surface displacement of a neighbouring active rock glacier located in the eastern Italian Alps. The photos were acquired in 2013 and 2014 using a digital consumer-grade camera during single-day field surveys. Airborne laser scanning (ALS, otherwise known as airborne lidar) data were used as benchmarks to estimate the accuracy of the photogrammetric digital elevation models (DEMs) and the reliability of the method. The SfM–MVS approach enabled the reconstruction of high-quality DEMs, which provided estimates of glacial and periglacial processes similar to those achievable using ALS. In stable bedrock areas outside the glacier, the mean and the standard deviation of the elevation difference between the SfM–MVS DEM and the ALS DEM was -0.42 ± 1.72 and $0.03 \pm 0.74\,\mathrm{m}$ in 2013 and 2014, respectively. The overall pattern of elevation loss and gain on the glacier were similar with both methods, ranging between -5.53 and $+3.48\,\mathrm{m}$. In the rock glacier area, the elevation difference between the SfM–MVS DEM and the ALS DEM was $0.02 \pm 0.17\,\mathrm{m}$. The SfM–MVS was able to reproduce the patterns and the magnitudes of displacement of the rock glacier observed by the ALS, ranging between 0.00 and 0.48 m per year.

The use of natural targets as ground control points, the occurrence of shadowed and low-contrast areas, and in particular the suboptimal camera network geometry imposed by the morphology of the study area were the main factors affecting the accuracy of photogrammetric DEMs negatively. Technical improvements such as using an aerial platform and/or placing artificial targets could significantly improve the results but run the risk of being more demanding in terms of costs and logistics.

1 Introduction

Knowledge of changes in the extent, mass and surface velocity of glaciers and rock glaciers contributes to a better understanding of the dynamic processes occurring in cold high-mountain environments and serves as an important contribution to climate monitoring (Kääb et al., 2003). Numerous techniques exist for monitoring and quantifying these

changes, and such techniques include both field and remote sensing methods (Immerzeel et al., 2014). Fieldwork generally yields high-quality data but with a small spatial extent, given the remoteness and low accessibility of mountain areas at high elevations (Roer et al., 2007). Therefore, using remotely sensed data sets for at least two different points in time has become an important tool for monitoring high-mountain terrain dynamics (Kääb, 2002). Multitemporal dig-
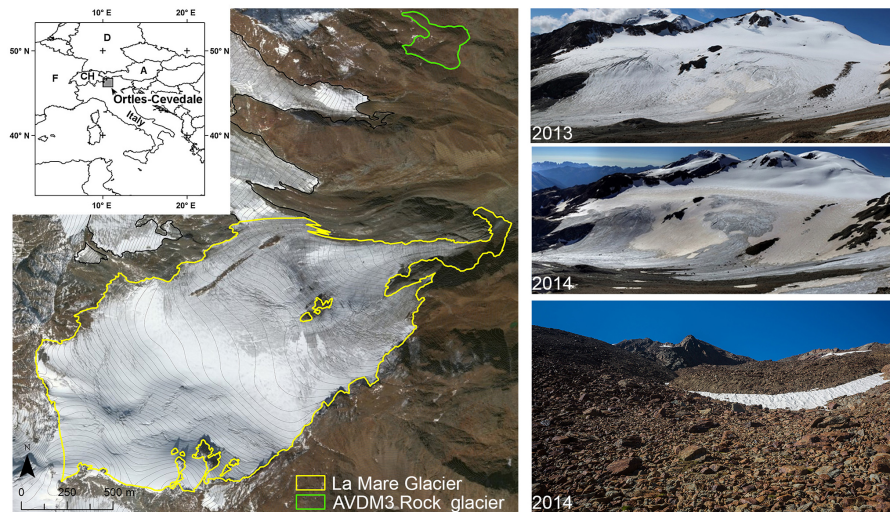
Figure 1. Geographic setting of study areas. Panoramic view of the La Mare Glacier from the same camera position on 4 September 2013 and 27 September 2014. The lower right photograph shows the front of the meridional lobe of the AVDM3 Rock glacier, which was surveyed on 27 September 2014.

ital elevation models (DEMs) based on remote sensing data are the most commonly used products for such investigations (Kääb, 2005; Tseng et al., 2015).

Among the available remote sensing techniques, close-range photogrammetry has experienced a rapid development thanks to the recent progress in digital photogrammetry, based on computer vision algorithms. This technique is becoming the major alternative to traditional surveying techniques and lidar (light detection and ranging) technologies, due to its lower cost, high portability, and easy and rapid surveying in the field.

The photogrammetric approach known as structure from motion (SfM) allows 3-D information of the photographed object to be obtained from a sequence of overlapping images taken with a digital camera. There are only a limited number of examples where SfM photogrammetry has been applied in glacial and periglacial environments, and these studies principally involve the use of unmanned aerial vehicles (UAVs) for image acquisition (Solbø and Storvold, 2013; Whitehead et al., 2013; Immerzeel et al., 2014; Tonkin et al., 2014; Gauthier et al., 2014; Bühler et al., 2015; Dall'Asta et al., 2015; Ryan et al., 2015) rather than ground-based surveys (Gómez-Gutiérrez et al., 2014, 2015; Kääb et al., 2014; Piermattei et al., 2015).

The objective of our work is to assess the suitability of the ground-based SfM approach for monitoring glacial and periglacial processes in a high-altitude area of the Ortles–Cevedale Group (eastern Italian Alps). In particular, this approach was used to calculate the geodetic annual mass balance of a 2.1 km^2 glacier and to detect the surface displacement of a neighbouring 0.06 km^2 rock glacier. The photogrammetric surveys were intentionally planned to be as quick and cost-effective as possible and easily replicable in

the future. Therefore, a consumer-grade camera was used in order to strike an appropriate balance between (i) the affordability and accessibility of the system (i.e. cost and ease of use) and (ii) the quality of the resulting topographic data (accuracy and measurement density). The accuracy of the photogrammetric DEMs was assessed by comparison to airborne laser scanning (ALS) based DEMs acquired within 3 weeks or less of their survey. The main factors affecting the accuracy of the photogrammetric DEMs were investigated, and the significance of the biases in the quantification of glacial and periglacial processes was discussed.

2 Geographical setting and case studies

The La Mare Glacier and the neighbouring AVDM3 (Alta Val de la Mare, 3rd; Carturan et al., 2015) Rock glacier are located in the south-eastern part of the Ortles–Cevedale massif (eastern Italian Alps), the largest glaciated mountain group of the Italian Alps (Fig. 1).

The La Mare Glacier (World Glacier Inventory code I4L00102517; WGMS 1989) is a 3.55 km^2 valley glacier currently composed of two ice bodies, which have different morphologies and tend to separate (Carturan et al., 2014). In this work, the focus was on the southern ice body, which feeds the main tongue. This 2.1 km^2 ice body primarily faces north-east, and its surface is rather flat, with the exception of the small remnant of its valley tongue. The elevation ranges from 2660 to 3590 m a.s.l. Mass balance investigations using the glaciological method, based on in situ measurements of surface ablation and accumulation (Østrem and Brugman, 1991), were started on La Mare Glacier in 2003 and detected an average annual mass balance of −0.76 m water equiva-
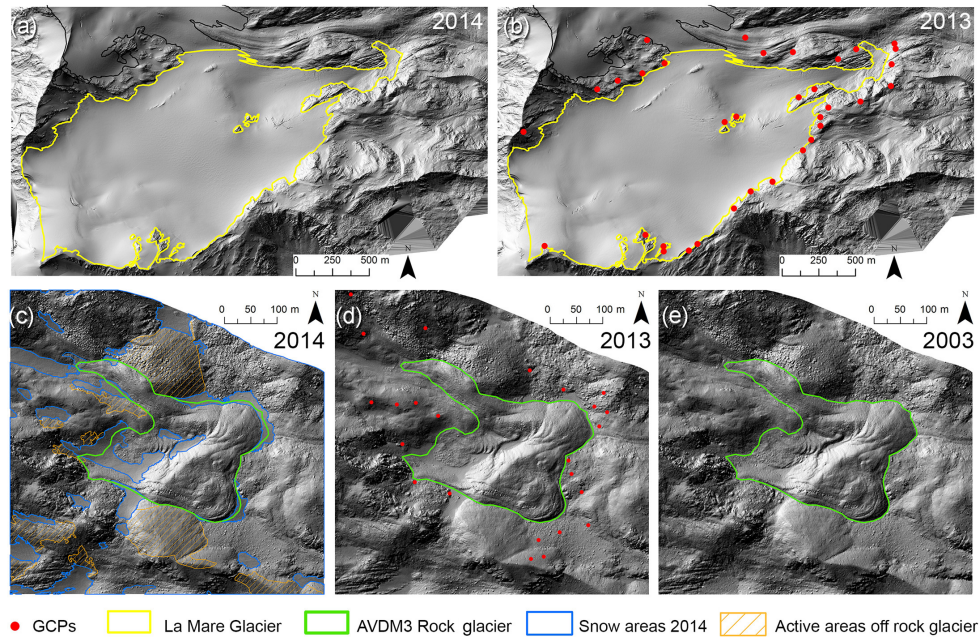
Figure 2. Hillshade of the ALS DEMs of La Mare Glacier acquired on **(a)** 24 September 2014 and **(b)** 21 September 2013. Hillshades of the ALS DEMs of rock glacier acquired in **(c)** 2014, **(d)** 2013 and **(e)** 2003.The red dots represent the selected ground control points (GCPs) in 2013 DEM used for the photogrammetric approach. The snow accumulation areas and the geomorphologically active areas outside the rock glacier were excluded during the ICP computation between 2013 and 2003, 2014 ALS point cloud.

lent per year (w.e. yr^{-1}) during the period from 2003 to 2014 (Carturan, 2016). The mass balance was close to 0 in 2013 (−0.06 m w.e.) and was positive for the first time since the beginning of measurements in 2014 (+0.83 m w.e.).

The AVDM3 Rock glacier (Carturan et al., 2015) is an intact, tongue-shaped rock glacier characterized by the presence of two lobes. The 0.058 km^2 wide rock glacier (maximum length of 390 m; maximum width of 240 m) faces south-east and is located at elevations of between 2943 and 3085 m a.s.l. The average slope of the rock glacier is 26°, and the slope of the advancing front is 36°. The activity status of the AVDM3 Rock glacier was assessed via repeated geomorphological field surveys between 2007 and 2014. These surveys revealed the advance of the front of the southern lobe (Carturan, 2010). The general morphology and the elevation of the front also suggest that this rock glacier is active (Seppi et al., 2012), and its state is further corroborated by spring temperature measurements (Carturan et al., 2015). Moreover, Bertone (2014) provided the first quantification of the surface displacement rates of this rock glacier from 2003 to 2013 using ALS data, with rates averaging 8 cm yr^{-1}.

3 Methods

3.1 The ALS data

ALS flights of the study area were available for 17 September 2003, 22 September 2013 and 24 September 2014. The

technical specifications of the three ALS surveys are reported in Table 1. To avoid errors due to global shifts or rotations between the individual DEMs, the ALS point clouds were automatically co-registered using a version of the Iterative Closest Point (ICP) algorithm (Chen and Medioni, 1991; Besl and McKay, 1992) tailored to topographic point clouds (OpalsICP algorithm from TU Wien, Glira et al., 2015). The lidar point cloud acquired in 2013 was treated as a reference only for stable areas outside the glaciers, rock glaciers, snow patches and geomorphologically active areas (e.g. landslides, river beds and debris flows). The 2003 and 2014 lidar point clouds were iteratively fitted to the reference point cloud by applying an ICP transformation. The ICP registration of the point clouds produced z-direction residual values of 0.08 and 0.11 m for the 2014 and 2003 lidar point clouds, respectively. These accuracies were found to be sufficient for calculating the annual elevation changes in the glacier and the decadal displacement rate on the rock glacier (Bertone, 2014; Carturan, 2016).

The co-registered point clouds were then converted to DEMs using natural neighbour interpolation. A pixel size of 1×1 m was produced for the La Mare Glacier, whereas a pixel size of 0.5×0.5 m was used for the rock glacier, based on the lidar point cloud density (Fig. 2). To evaluate the relative ALS DEM accuracies after the co-registration, the elevation difference errors of the DEMs were calculated for the stable areas. The standard deviation from the 2013 ALS

Table 1. Date and main parameters of available lidar data. The dash indicates that no information is available.

Date	Aircraft	Laser scanner model	Laser scanner rate	Max. scan angle	Scan frequency	Point density (pts m^{-2})
24 Sep 2014	Helicopter AS350 B3	Optech ALTM GEMINI (04SEN164)	100 kHz	46°	34 Hz	5.1
22 Sep 2013	Cessna 404 D-IDOS	ALTM 3100	70 kHz	±25°	32 Hz	0.9
17 Sep 2003	–	–	–	–	–	0.5
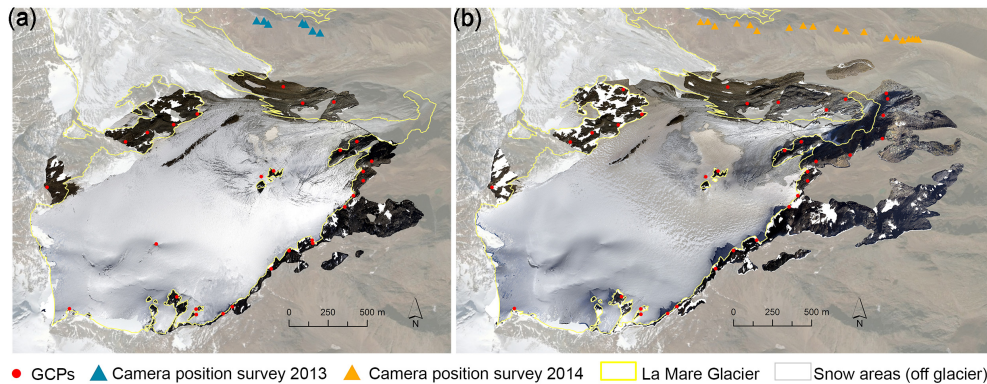
Figure 3. Orthophotos derived from the SfM–MVS 3-D model of La Mare Glacier surveyed on **(a)** 4 September 2013 and **(b)** 27 September 2014. The white areas in the orthoimages represent the snow-covered area in the rock stable area. The red dots outside the glacier area are the GCPs and the triangles are the identified camera locations.

DEM was 0.19 and 0.21 m for the 2014 and 2003 DEM comparisons, respectively.

3.2 The photogrammetric workflow

3.2.1 Field surveys

The terrestrial photogrammetric surveys of the La Mare Glacier were conducted on 4 September 2013 and 27 September 2014, that is, close to the end of the mass balance year and the ALS flights. The timing of the surveys enabled the calculation of the annual mass balance of the glacier and the comparison of the results with the ALS-based results. On both days, the sky was clear, with almost no cloud cover.

To guarantee a safe and easily repeatable survey of the glacier, direct access to its surface was avoided and the survey was performed from a rocky ridge on the north side of the glacier (Fig. 5). The elevation of the camera positions ranged from 3100 to 3300 m in 2013 and from 2600 to 3300 m in 2014. The distance from the glacier surface to the camera positions dictated by the topography ranged between 300 and 2900 m. To cover the entire glacier surface from these positions, the acquired images were panoramic, which involved taking a series of photographs rotating the camera from each individual camera position. In 2013, seven camera positions were used, and 37 photographs were taken with the camera attached to a small tripod to avoid camera shake. In 2014,

the number of camera positions was increased to 21, and 177 photos were taken freehand (Fig. 3, Table 2).

Both surveys were performed in the morning, avoiding the hours with too high a solar zenith angle (Table 2), using an SLR Canon EOS 600D. The camera was equipped with a 25–70 mm zoom lens, which was set to a focal length of 25 mm in 2013 and 35 mm in 2014.

The terrestrial photogrammetric survey of the AVDM3 Rock glacier was performed on 27 September 2014, between 12:15 and 14:00 LST (local solar time). In this survey, 198 images were acquired freehand while walking around and on top of the rock glacier. The survey camera was a CANON EOS 5D full frame SLR camera equipped with a fixed-focal lens of 28 mm. The photographs were acquired and saved in raw file format in both surveys.

3.2.2 Data processing

The photogrammetric approach, based on SfM algorithms, can automatically derive the 3-D position of an object in images taken in sequence calculating the camera parameters (intrinsic and extrinsic) (Hartley and Zissermann, 2003). Dense image matching algorithms are then used to reconstruct the 3-D model of the object as a dense point cloud. Multiple photogrammetric packages implementing SfM and multi-view stereo (MVS) algorithms for dense image matching exist, and in this work, the software PhotoScan Pro (AgiSoft LLC, 2010a) was used. Henceforth, the photogram-

Table 2. Data acquisition settings and processing results of the photogrammetric surveys for both case studies. The GCP error is the average transformation residual error (m) and root mean square reprojection error for the GCPs (pix) during the bundle adjustment computation. The image quality refers to the downsampling of the image resolution during the dense matching computation. "Ultra high" means full resolution and "high" a downsampling of 50 % before image matching procedure. The ground sample distance (GSD) is the average pixel size on the ground. The standard deviation of the ICP (Iterative Closest Point) registration is reported in the table.

	La Mare Glacier		Rock glacier
	4 Sep 2013	27 Sep 2014	27 Sep 2014
Input data			
Camera type	Nikon 600D	Nikon 600D	Canon 5D Mark III
Focal length	25 mm	35 mm	28 mm
Image size	5184 × 3456 pix	5184 × 3456 pix	5760 × 3840 pix
No images	37	177	198
Acquisition time	10:10–12:00	7:50–10:40	12:15–14:00
Processing data			
Reprojection error	0.43 pix (1.76 max)	0.40 pix (3.75 max)	0.38 pix (1.20 max)
GCP error	1.52 m 1.48 pix	1.14 m 1.96 pix	0.62 m 1.86 pix
Image quality	Ultra high	High	High
Mean GSD	0.16 m pix^{-1}	0.22 m pix^{-1}	0.064 m pix^{-1}
Dense point cloud	49, 844, 094 pts	55, 114, 074 pts	56, 171, 705 pts
Point density	37 pts m^{-2}	20 pts m^{-2}	244 pts m^{-2}
Post-processing data			
Filtered point cloud /subsampled	15, 617, 342 pts (sampled 0.20 m)	24, 226, 221 pts (sampled 0.20 m)	4, 517, 143 pts (sampled 0.10 m)
Point density	8 pts m^{-2}	9 pts m^{-2}	21 pts m^{-2}
ICP transformation	0.14 m	0.15 m	0.10 m

metric surveys and results are referred to using the acronym SfM–MVS.

The photo-based reconstruction workflow is summarized in Fig. 4. The key components of the workflow are (1) acquisition and photograph editing, (2) ground control point (GCP) identification, image feature detection, matching and 3-D scene reproduction (the SfM–MVS steps), (3) point cloud processing (filtering, subsampling and ICP) and (4) DEM reconstruction.

To overcome the significant variability in brightness during the surveys, the raw-format images have been edited to adjust the exposure and contrast in order to retrieve information from the overexposed (e.g. snow-covered) areas and underexposed (e.g. shadowed) areas. These editing steps had a positive impact on the number of image features extracted. The edited images were saved in TIFF format and loaded in PhotoScan where nonstationary objects (i.e. clouds and shadows), the sky and features lying in the distant background have been masked.

The camera calibration parameters were calculated prior to the processing of the photogrammetric surveys. The camera was calibrated in a field test area, using artificial targets surveyed by total station and maintaining the same camera setting adopted during the photogrammetric surveys. The calculated intrinsic parameters were kept constant during the bundle adjustment optimization (Triggs et al., 1999) given the limits of the camera network geometry and the homogeneous texture of the surveyed terrain. As additional constraint, GCPs were included into the SfM process to avoid instability in the bundle adjustment solution (Verhoeven et al., 2015). The GCPs were selected to be natural features in stable areas outside the glacier and rock glacier, and their coordinates were extracted from the 2013 ALS hillshaded DEM. After the SfM step, the geo-referenced dense point cloud was reconstructed by the MVS algorithm, using the "mild" smoothing filter to preserve as much spatial information as possible (AgiSoft LLC., 2010b).

To reduce the noise and outliers generated during the dense matching reconstruction (Bradley et al., 2008; Nilosek et al., 2012), an initial filtering was performed in PhotoScan to manually remove the outliers. Further denoising was applied to the dense point clouds exported from PhotoScan, using a tool implemented in the open-source software CloudCompare, based on the statistical approach called S.O.R. (statistical outlier removal). To obtain a uniform spatial distribution of the points, the photogrammetric point clouds (much denser than the ALS point clouds), were downsampled to 20 cm for the glacier and 10 cm for the rock glacier, using the spatial subsampling tool of CloudCompare. Following the same procedure used for the ALS data, the ICP algorithm was applied to co-register the point clouds in the stable area outside the glacier and rock glacier, using the 2013 ALS point cloud as a reference. The co-registered point clouds were then converted to DEMs, using natural neighbour interpolation and the same pixel sizes as the ALS DEMs (i.e. 1 × 1 m for the glacier and 0.5 × 0.5 m for the rock glacier).
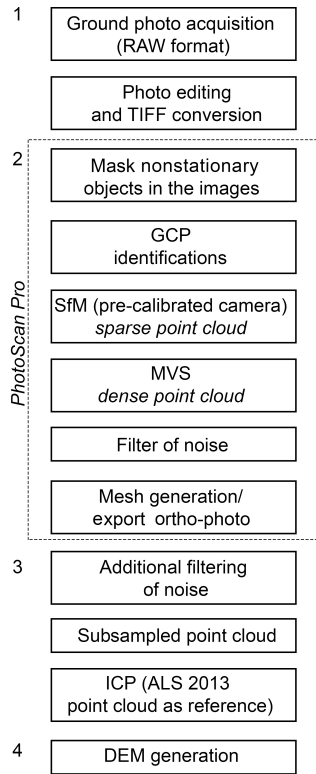
Figure 4. Workflow illustrating the photo-based 3-D reconstruction process used in this work for both case studies, starting from image collection through the DEM generation.

The data acquisition settings and processing results of the photogrammetric surveys are summarized in Table 2.

3.3 Analyses

The accuracy of the photogrammetric DEMs was assessed by calculating the mean, the mean of the absolute values and the standard deviation (σ) of the elevation differences (DEM of difference, DoD) between SfM–MVS DEMs and ALS DEMs, using the latter as a reference data set. For both surveyed areas, the primary factors controlling the quality of the photogrammetric results were evaluated in terms of DEM accuracy and spatial resolution. For the La Mare Glacier area, the role of slope, angle of incidence, camera–object distance, camera network geometry and surface texture was analysed. The role of the incidence angle between the line of sight of the camera and the photographed object (vector normal to the surface), was investigated by analysing the mean angles calculated from five representative camera locations at different elevations. Because the redundancy of the observations, that is the number of cameras that view the same point on the glacier, influences the quality of the photogrammetric results, a viewshed analysis was carried out calculating the number of cameras able to see each pixel. The effect of the

camera–object distance (i.e. depth; Gómez-Gutiérrez et al., 2014), was evaluated by calculating the accuracy for pixels clustered at 200 m distance classes from a camera position at the centre of the array displayed in Fig. 5b. The obtained results were compared to the theoretical behaviour of the error as a function of the depth (σ_d), calculated using the following formulation:

$$\sigma_d = m_B \cdot \frac{D}{B} \cdot \sigma_i, \tag{1}$$

where m_B represents the image scale (D/focal length), D is the depth (camera–object distance), B is the baseline (i.e. the distance between each pair of adjacent camera positions) and σ_i is the measured accuracy in the image space. The accuracy of photogrammetric reconstructions for the different substrata was then evaluated, outlining each substratum on the orthophoto exported from PhotoScan.

For the rock glacier area, only the effect of slope and shadow areas on the accuracy of the SfM DEM was evaluated, as others factors like the camera–object distance and the incidence angle cannot be reliably quantified due to the different ground survey characteristics (i.e. the photos were acquired by walking on the target). As suggested by Gómez-Gutiérrez et al. (2014), the relationship between the quality of the photogrammetric DEM and the amount of shadowed–lighted areas in the photographs was calculated using a hill-shaded model that was calculated by simulating the azimuth and zenith angles of the sun in the sky during the survey (astronomical applications tool). After the accuracy assessments, we investigated the suitability of using the terrestrial photogrammetric surveys to calculate the annual mass balance of the glacier and the surface displacement rates of the rock glacier, comparing the results with those obtained from ALS surveys. The mass balance and elevation changes were calculated by differencing multitemporal DEMs.

The geodetic mass balance was calculated from the total volume change ΔV (m^3) of the glacier between two survey dates:

$$\Delta V = \overline{\Delta z} \cdot A, \tag{2}$$

where $\overline{\Delta z}$ is the average elevation change between two DEMs over the area A of the glacier. The area-averaged net geodetic mass balance in metres of water equivalent per year (m w.e. yr^{-1}) was calculated as:

$$\dot{M} = \frac{\Delta V \cdot \rho}{A}, \tag{3}$$

where ρ is the mean density, obtained by a fractional area-weighted mean, assigning 900 kg m^{-3} for the ablation area (Huss, 2013) and 530 kg m^{-3} for the accumulation area, as directly measured in a snow pit. The resulting weighted mean density was 600 kg m^{-3}. The area A of the glacier between the two surveys did not change. In the mass balance calculations, we used both raw $\overline{\Delta z}$ values and $\overline{\Delta z}$ values corrected
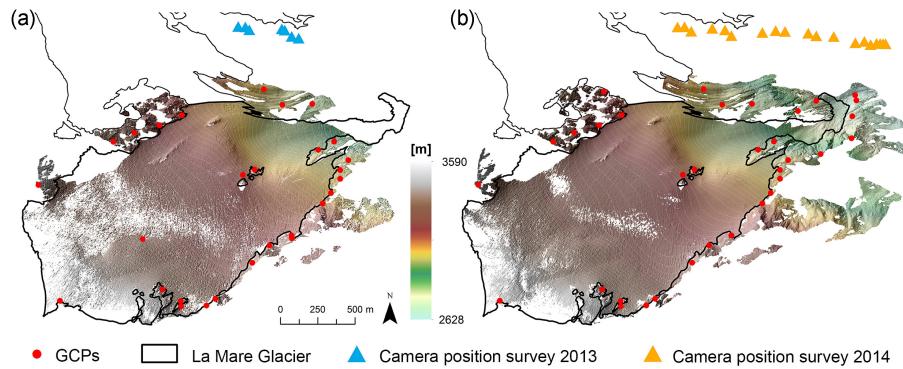
Figure 5. Hillshaded DEMs with superposed semi-transparent colour map of La Mare Glacier derived from photogrammetric measurements for **(a)** 4 September 2013 and **(b)** 27 September 2014 image surveys.
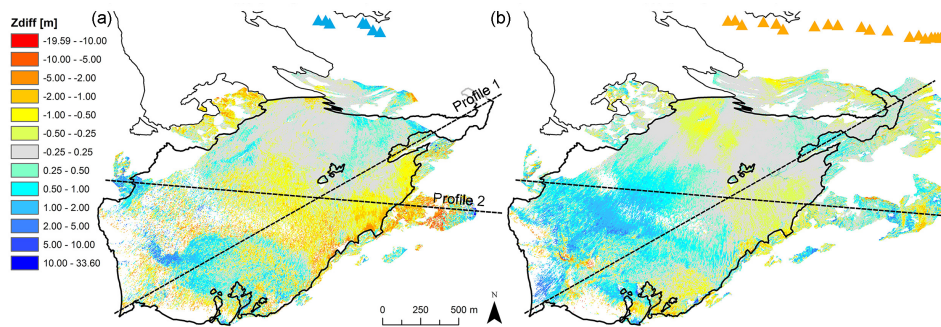
Figure 6. Spatial distribution of elevation differences between photogrammetric and ALS-based DEMs for **(a)** 2013 and **(b)** 2014. Black lines are the location of profiles in Fig. 7.

by removing the mean error in the stable areas outside the glacier (Table 3). Other processes like ice fluxes, varying snow density and refreezing of meltwater were assumed to be negligible for the calculation of the annual geodetic mass balance (Zemp et al., 2013).

The horizontal surface displacements rates of the AVDM3 Rock glacier were estimated by a manual measurement of the displacement of single boulders identified in the hillshaded DEMs. Several points were also located outside the rock glacier to assess the accuracy of the surface velocity determinations. Displacements in the horizontal plane were analysed instead of 3-D displacements, which are affected by surface elevation changes (Isaksen et al., 2000).

4 Results

4.1 Accuracy assessment on the area of La Mare Glacier

The mean elevation difference between the SfM–MVS DEM from 4 September 2013 (Fig. 5a) and the ALS DEM from 22 September 2013 (Fig. 2b), evaluated in the common stable area outside the glacier, was -0.42 m ($\sigma = 1.72$ m). The same calculation between the SfM–MVS DEM from 27 September 2014 (Fig. 5b) and the ALS DEM from 24 September 2014 (Fig. 2a) yielded a mean value of 0.03 m ($\sigma = 0.74$ m). In this area, the mean difference between the 2014 and 2013 SfM–MVS DEMs is 0.38 m ($\sigma = 1.73$ m), and the mean difference between the respective ALS DEMs is -0.09 m ($\sigma = 0.29$ m, Table 3).

These results show that the photogrammetric survey conducted in 2014, using a higher number of camera positions and photographs and a slightly longer focal length, provided a significant improvement compared to the survey of 2013. In addition to the higher σ, the 2013 SfM–MVS DEM has a residual average bias of -0.42 m, which must be taken into account in the glacier mass balance calculations. Table 3 presents the same statistics for the data covering the glacier. However, given that in 2013 the ablation was not negligible between the photogrammetric survey of 4 September and the ALS survey of 22 September, the comparison between SfM–MVS and ALS of the same year is meaningful only in 2014, with a mean difference of 0.23 m ($\sigma = 0.65$ m).

The spatial distribution of the elevation difference between the SfM–MVS and ALS DEMs surveyed at the same time (Figs. 6 and 7) suggests that the most problematic areas for photogrammetric reconstructions are those that are far from the camera positions, steep and covered by fresh snow.

Table 3. Comparison between SfM–MVS-based DEMs and ALS-based DEMs in the common area outside and inside the La Mare Glacier.

DEMs			Elevation differences (m) cell size 1 m × 1 m							
			Common SfM–MVS bare-ground area				Common SfM–MVS glacier area			
			Min	Max	Mean	σ	Min	Max	Mean	σ
SfM–MVS 2013	vs.	ALS 2013	−19.59	33.61	−0.42	1.72	−9.91	12.04	−0.13	0.78
SfM–MVS 2014	vs.	ALS 2014	−18.48	22.42	0.03	0.74	−18.17	11.41	0.23	0.65
SfM–MVS 2014	vs.	SfM–MVS 2013	−33.12	14.19	0.38	1.73	−12.44	12.33	1.58	1.42
ALS 2014	vs.	ALS 2013	−15.38	10.81	−0.09	0.29	−14.61	7.37	1.30	0.97
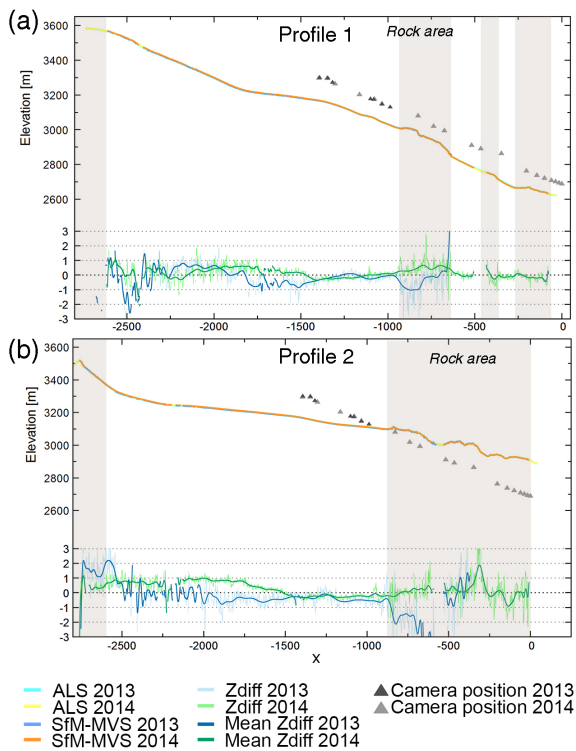
Figure 7. Cross sections through the La Mare Glacier DEMs show the glacier elevation change and the difference between 2013 and 2014 in SfM–MVS and ALS-based DEMs. The location of **(a)** profile 1 and **(b)** profile 2 is indicated in Fig. 6. The x axis zero has been fixed at the first camera position of the 2014 survey and the minimum and maximum values of the z-difference set to ±3 m and both profiles and the camera positions were projected onto the xz plain. The shaded area represent bare-ground stable areas.

Certain outliers can be observed in steep areas outside the glaciers, even after filtering, but they likely have no influence on the glacier, where the slope is much lower.

The factors controlling the quality of the photogrammetric DEMs were investigated in detail using the SfM–MVS DEM from 27 September 2014, which has a higher spatial coverage than that of 2013 and is almost contemporaneous with the ALS DEM from 24 September 2014 (which means negligible ablation and accumulation on the glacier).

As expected, the standard deviation of elevation differences between the 2014 SfM–MVS and ALS DEMs is proportional to slope but remains lower than 1 m up to 40° on the glacier and up to 60° in the area outside it (Fig. 8). Grouping the data for slope classes of 10° and excluding classes with less than 1000 grid cells, a positive correlation was found between the absolute value of the elevation difference and the slope ($R = 0.86$ both inside and outside the glacier, significant at the 0.05 level). A rapid increase in the error is observed for the highest slope classes, which represent a very small proportion of the investigated area. For the glacier, only 1 % of the area has a slope higher than 40°. The mean elevation difference is around 0 for most of the low- and middle-slope classes, with the exception of the 0–10° class inside the glacier, where a mean value of 0.41 m ($\sigma = 0.44$ m) was calculated. Interestingly, the majority of this slope class lies in a flat area of the glacier at 3200–3300 m a.s.l. and is covered by fresh snow, which has poor texture. In addition, this zone has an unfavourable line of sight from the camera positions.

In the glacier area most of the mean incidence angles range between 70 and 90° (75 %, Fig. 9a). The scatter plot of elevation differences between the 2014 SfM–MVS and ALS DEMs versus the mean incidence angles calculated for every pixel shows no statistically significant relationship ($R = 0.21$). However, analysing this relationship for classes of incidence angle and considering the mean of the elevation differences in absolute value and the classes with more than 1000 pixels yields a correlation coefficient $R = 0.95$ (significant at the 0.05 level).

The results of the viewshed analysis (Fig. 9d) show anti-correlation between the absolute value of elevation difference and the number of cameras viewing reconstructed pixels (Fig. 9e), yielding a coefficient of correlation of −0.63, which is significant at the 0.05 level.

The relationship between error and depth is clearer for the glacier area (Fig. 10a), whereas in the surrounding bare-ground area, the error appears to be more influenced by the variability in the slope angle (Fig. 10b).

The theoretical σ_d was calculated using Eq. (1) for each class of distance, considering a mean baseline of 400 m and an accuracy in the image space of 0.40 pixel, which is the reprojection error after bundle adjustment. Another quantifi-
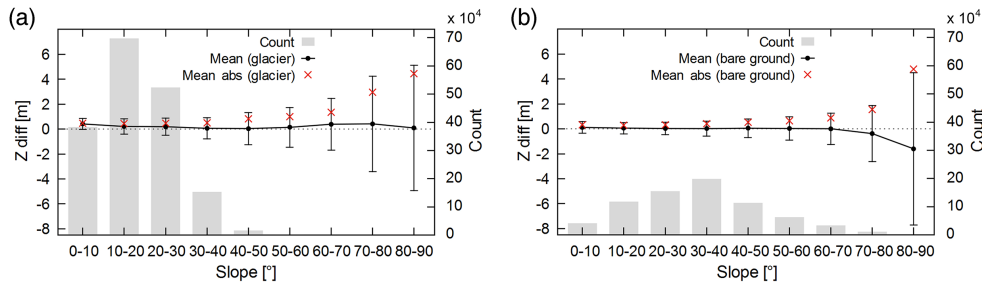
Figure 8. Mean, mean of the absolute values and standard deviation of the 2014 DoD between SfM–MVS and ALS-based DEM depending on slope calculated **(a)** inside the glacier area and **(b)** in the bare ground outside glacier covered by rock. The grey bars show the count of cells at any given slope (y axis on the right).
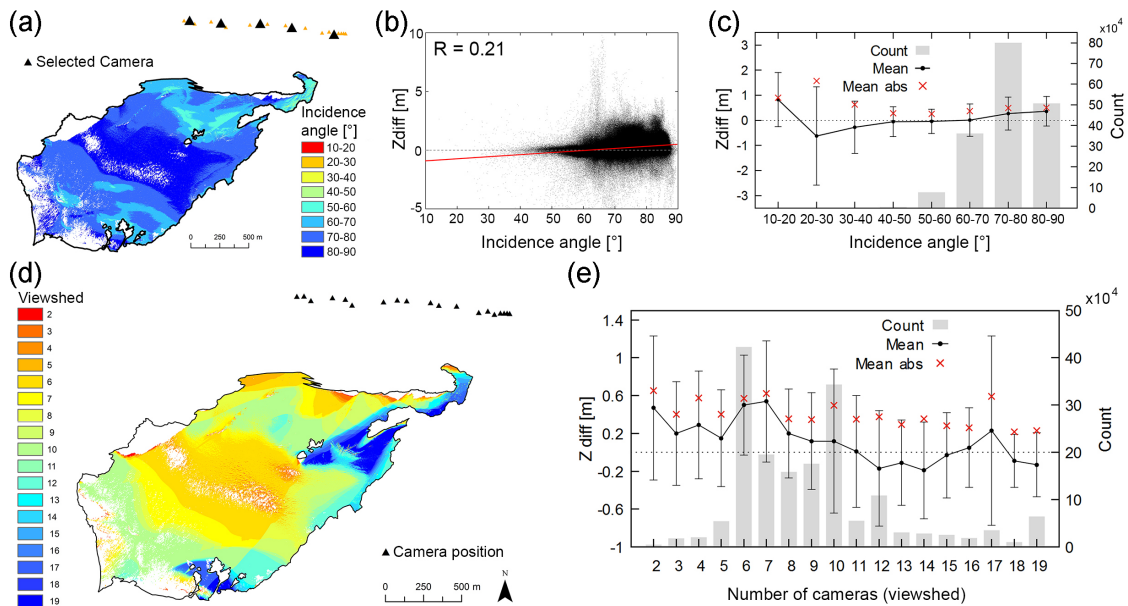
Figure 9. Mean incidence angles between five representative cameras positions and vectors normal to the surface and viewshed analysis: **(a)** map of the mean incidence angle calculated for five representative camera positions; **(b)** the scatter plot of the elevation difference and the mean incidence angle for the five representative camera positions; **(c)** mean with 1 standard deviation error bars in y and mean of the absolute value of elevation differences for the mean incidence angle intervals calculated for the five selected representative camera positions, in $10°$ bins; **(d)** map of the analysis using viewshed number of cameras able to see each pixel derived from all camera positions; **(e)** mean with 1 standard deviation error bars and mean of the absolute value of elevation differences for the viewshed reconstructed area analysis.

cation of the error as a function of the depth was obtained, for comparison purposes, by multiplying the ground sample distance (GSD) (which increases with depth) by the reprojection error provided by PhotoScan for the ground control points. Figure 10c shows that, on the glacier, the accuracy calculated from the DoD matches the theoretical calculations up to a depth of 1900 m quite well. Beyond this distance, the detected error increases faster than in theory, likely due to the increasing coverage of fresh snow, which affects the image texture and decreases the accuracy.

Debris-, ice- and firn-covered areas display similar accuracy, with median values of elevation difference between the 2014 SfM–MVS and ALS-based DEMs close to zero and interquartile ranges of the same magnitude (Fig. 11). Conversely, the area covered by fresh snow, which is also the area with greater depth, shows overall positive differences, a median value of 0.48 m and a much higher standard deviation ($\sigma = 0.82\,\mathrm{m}$).

The texture of the surface also influences the point density distribution and the spatial coverage of the reconstructed area. A lower value of the point density was obtained for fresh snow (4 pts m^{-2}). Increasing point densities were obtained for firn, ice and debris (10, 13 and 15 pts m^{-2}, respectively). The spatial coverage in the fresh-snow area was 75 %, whereas it was 93 % in the rest of the glacier. Excluding the areas not visible from the camera position and occlu-

Table 4. Mass balance calculations on La Mare Glacier using different combinations of SfM–MVS and ALS DEMs.

DEMs cell size 10 m			Spatial coverage (m^2)	Average elevation changes (m)		Volume change (m^3)		Mass balance (m w.e.)	
			Mass balance estimation	Raw	Corrected	Raw	Corrected	Raw	Corrected
SfM–MVS 2014	vs.	SfM–MVS 2013	1 834 800 (∼ 88 %)	1.81	1.45	3 320 988	2 660 460	1.09	0.87 ± 1.30
ALS 2014	vs.	ALS 2013		1.47	1.56	2 697 156	2 862 288	0.88	0.94 ± 0.16
SfM–MVS 2014	vs.	ALS 2013	1 938 700 (∼ 93 %)	1.64	1.70	3 179 468	3 295 790	0.98	1.02 ± 0.60
ALS 2014	vs.	ALS 2013		1.41	1.50	2 733 567	2 908 050	0.85	0.90 ± 0.16
ALS 2014	vs.	ALS 2013	2 072 700 (entire glacier)	1.43	1.52	2 963 961	3 150 504	0.86	0.91 ± 0.16

Table 5. Statistics of elevation changes in the rock glacier and in bare-ground stable area outside the rock glacier from September 2014 to September 2013 and from September 2003 in the ALS reconstructed area and in the common ALS and SfM–MVS coverage area.

DEMs			Elevation changes (m)							
			ALS reconstructed area				SfM–MVS reconstructed area			
			Stable area		Rock glacier		Stable area		Rock glacier	
			Mean	σ	Mean	σ	Mean	σ	Mean	σ
SfM–MVS 2014	vs.	ALS 2014	–	–	–	–	0.05	0.31	0.02	0.17
SfM–MVS 2014	vs.	ALS 2013	–	–	–	–	0.01	0.33	−0.04	0.18
ALS 2014	vs.	ALS 2013	−0.05	0.19	−0.07	0.12	−0.05	0.20	−0.07	0.12
SfM–MVS 2014	vs.	ALS 2003	–	–	–	–	0.06	0.33	−0.16	0.49
ALS 2014	vs.	ALS 2003	−0.01	0.22	−0.18	0.46	−0.00	0.21	−0.18	0.47
ALS 2013	vs.	ALS 2003	0.04	0.21	−0.11	0.41	–	–	–	–

sions imposed by the topography, the spatial coverage in the fresh-snow area was 82 and 98 % in the remaining part.

The point density is also affected by the depth, elevation and slope (Fig. 12). Due to the GSD, the average point density decreases with depth, which in our case is also proportional to the elevation. On the glacier, the point density decreases more rapidly than in the surrounding area for elevations between 3100 and 3300 m a.s.l., due to the poor texture in this snow-covered flat area. Increasing densities with slope, up to 70–80°, are observed and likely result from more favourable incidence angles, which do not however guarantee high accuracy, as noted earlier (Fig. 9). Considering the entire reconstructed surface, the point density was higher in the area surrounding the glacier than on it (12 pts m^{-2} vs. 8 pts m^{-2}, respectively).

4.2　Accuracy assessment in the area of the AVDM3 Rock glacier

The 2014 terrestrial photogrammetric survey of the AVDM3 Rock glacier provided a good spatial coverage (83 %) of high-resolution terrain data (Fig. 13). The spatial distribution of the elevation difference between the contemporaneous SfM–MVS and ALS DEMs shows the existence of areas with both positive and negative values (Fig. 14). The average

elevation difference is 0.02 m on the rock glacier ($\sigma = 0.17$) and 0.05 in the surrounding areas ($\sigma = 0.31$ m; Table 5).

Similar to the La Mare Glacier area, the accuracy decreases with increasing slope in the rock glacier area. The standard deviation of the average elevation difference between the SfM–MVS and ALS DEMs is less than 0.20 m up to 40° (Fig. 15a). In the area surrounding the rock glacier, the error increases faster with slope because steep areas coincide with shaded areas and (because the images were acquired in the afternoon) high solar zenith angles (Fig. 15b). Larger errors, indeed, occur in shadowed rather than in well-lit areas, even if the largest differences in accuracy can be observed outside rather than on the rock glacier (Fig. 16).

4.3　Glacial and periglacial processes
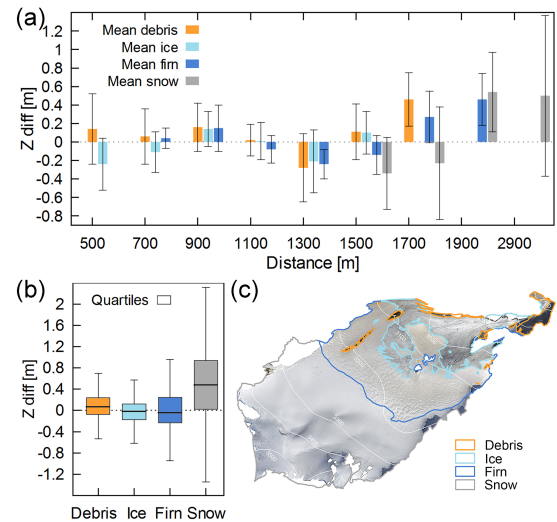
4.3.1　Mass balance of La Mare Glacier

Due to abundant solid precipitation during the accumulation season and low ablation rates during the summer (the glacier was snow-covered above ∼ 3000–3100 m a.s.l.), the mass balance of the La Mare Glacier was positive in the 2013–14 hydrological year for the first time since the beginning of measurements in 2003. The comparison of the two ALS DEMs of 2014 and 2013 yields a mean difference of
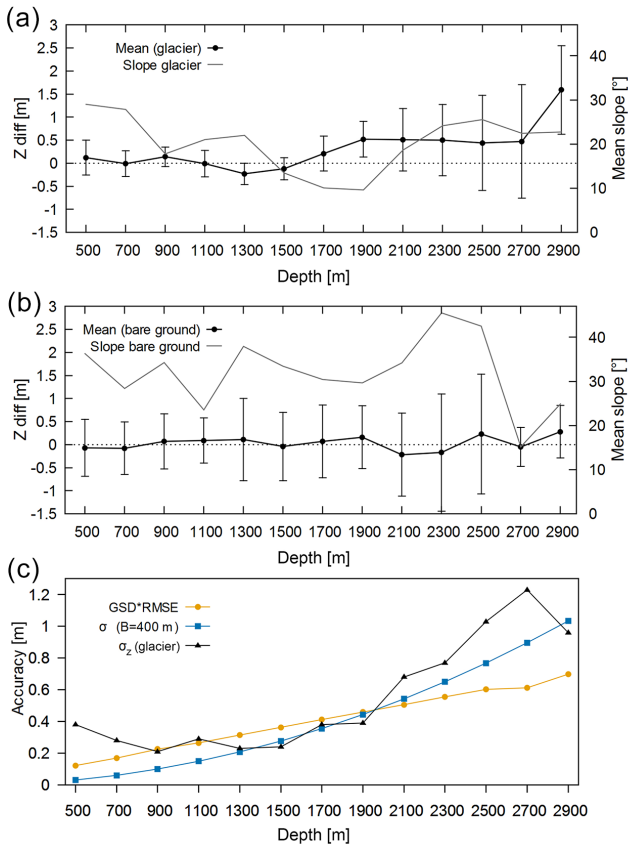
Figure 10. Mean and standard deviation of the 2014 DoD between SfM–MVS and ALS-based DEM depending on the distance from the camera depth (a) within the glacier area and (b) in the bare ground outside the glacier covered by rock. The trend of the average slope angle for each depth interval is shown on the right y axis. Panel (c): comparison of σ_z measured within the glacier area, the theoretical depth accuracy estimated according to Eq. (1) and the GSD multiplied by the GCP RMSE for each depth interval.

Figure 11. Elevation difference between the 2014 SfM–MVS and ALS-based DEMs calculated for different substrata. The figure shows (a) the mean and standard deviation of z difference for four substrata (debris, ice, firn and snow) grouped by distance from camera position and (b) the box plot of the z difference for four substrata. In the box–whisker plot, values which exceed $1.5 \cdot \mathrm{IQR}$ (interquartile range) were considered outliers. Panel (c): the orthophoto of the glacier on 27 September 2014 and map of substrata.

1.30 m for the glacier area, attributable to the positive annual mass balance measured by using the glaciological method in that time period (+0.83 m w.e.; Carturan, 2016).

As shown in Table 4, the geodetic mass balance estimates using only ALS data do not differ significantly for either the entire glacier or the subareas covered by the photogrammetric surveys of 2013 and 2014 (88 and 93 %, respectively). The estimates range between 0.85 and 0.88 m w.e. for the raw data and between 0.90 and 0.94 m w.e. for the corrected data. The geodetic mass balance calculations using only photogrammetric data yield a raw value of 1.09 m w.e. and a corrected value of 0.87 m w.e. Using the 2014 SfM–MVS, which has a higher quality than the 2013 SfM–MVS DEM, yields a raw value of 0.98 m w.e. and a corrected value of 1.02 m w.e. Area-averaged estimates of the geodetic mass balance from photogrammetric data are very close to the estimates from ALS data and from the glaciological method and are closer still if the mean DEM error in the stable areas outside the

glacier is subtracted from the raw average elevation differences. The spatial distribution and magnitude of elevation change is also well captured by the terrestrial photogrammetry (Figs. 17 and 18), even if, as already noted in the previous section, problematic areas are present in the upper part of the glacier, which was covered by fresh snow, especially in the 2013 SfM–MVS survey.

4.3.2 Surface changes and velocities of the AVDM3 Rock glacier

The spatial distribution and the mean value of elevation change on the surface of the AVDM3 Rock glacier were calculated differencing the available SfM–MVS and ALS DEMs. Table 5 shows that, according to the ALS data, there was an overall lowering of the surface in the period from 2003 to 2014. Taking into account the average residual bias in the stable area outside the rock glacier, the average lowering rates of the rock glacier surface were $1.5 \mathrm{\,cm\,yr^{-1}}$ in the period from 2003 to 2013 and 2 cm in the year 2013–14. Comparing the SfM–MVS DEM of 2014 with the ALS DEMs of 2013 and 2003 and accounting for the mean bias outside the rock glacier, we obtained slightly higher lowering rates of $2.2 \mathrm{\,cm\,yr^{-1}}$ from 2003 to 2013 and 5 cm from 2013 to 2014. As expected on the basis of the accuracy assessment (Sect. 4.2), the decadal lowering rates calculated from the SfM–MVS DEM are in closer agreement with those calculated from ALS data than the single-year calculations.

Table 6. Velocity statistics in three distinct areas of the rock glacier and in the stable area outside the rock glacier evaluated comparing the 2003 and 2014 ALS DEMs and the photogrammetric DEM for the 2014 survey epoch.

| | Horizontal movements between 2003 and 2014 (cm yr^{-1}) | | | | | | | | |
| | ALS 2003 vs. ALS 2014 | | | | | ALS 2003 vs. SfM–MVS 2014 | | | |
	No. points	Min	Max	Mean	σ	No. points	Min	Max	Mean	σ
Area 1	41	7.3	43.3	26.8	8.9	36	6.8	47.5	26.3	10.3
Area 2	13	4.4	27.4	18.9	7.0	11	9.0	27.9	18.1	6.4
Area 3	26	4.5	16.5	9.4	4.0	24	4.5	18.2	9.0	4.1
Off rock glacier	65	0.0	10.7	3.6	3.1	23	0.0	13.6	5.3	4.2
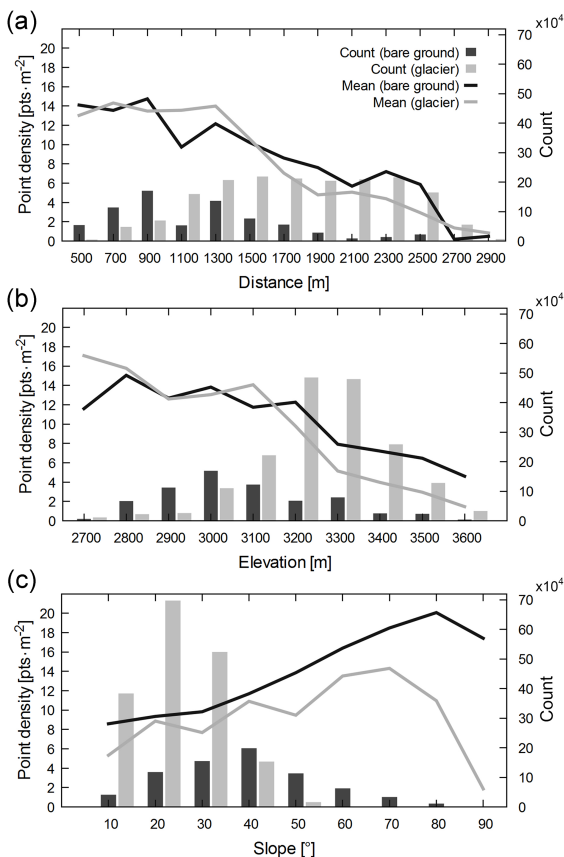
Figure 12. Relationships between point density of the 2014 photogrammetric 3-D model and **(a)** camera–object distance, **(b)** elevation and **(c)** slope calculated for the glacier and rock stable area outside glacier. The point density was estimated using the filtered and subsampled point cloud.

The same can be observed for the spatial distribution of the elevation changes (Fig. 19), which shows an overall thinning in the upper and middle part of the rock glacier and a thickening of the two advancing lobes. Figure 20 shows that the fastest moving areas in the period from 2003 to 2014 were the two frontal lobes, which also featured the greatest elevation

changes. Table 6 shows that the SfM–MVS and ALS data produced very similar surface velocities (ranging between 0.09 and 0.27 m yr^{-1} on average) for the three subareas, with homogeneous displacement, into which the rock glacier can be divided. Outside the rock glacier, the photogrammetric method exhibited a slightly lower accuracy compared to the ALS, but no systematic shift of the different DEMs was found.

5   Discussion

5.1   Data processing and accuracy assessments

The results of our terrestrial photogrammetry applications on the La Mare Glacier and on the AVDM3 Rock glacier demonstrate that it is possible to reliably quantify the investigated glacial and periglacial processes by means of a quick and safe survey that was conducted on a single day using cheap, light and easy-to-use hardware. Moreover, time-consuming and unsafe direct access to the glacier surface was not required. However, it should be noted that, without lidar data coverage, more time should have been invested in surveying GCPs and possibly placing artificial markers. The data processing did take a long time, however. For a single operator, the processing time is approximately 10 days, which is around twice the time necessary for lidar data processing. The most labour-intensive and time-consuming tasks were the pre-processing steps, i.e. the masking of the photos, identification of reference points from the lidar DEM and then in the images, and processing of the images (the MVS step is particularly computationally intensive), which is directly related to the resolution and the number of photographs uploaded and the computer performance. Several steps required a certain degree of subjectivity, e.g. the identification of the GCPs. However, due to the high automatism of the image processing, the level of expertise is considerably lower than for lidar and traditional photogrammetry.

On the La Mare Glacier, the area-averaged estimates of the 2013–14 geodetic mass balance from ALS and photogrammetric data were almost identical (0.91 ± 0.16 and 0.87 ± 1.30 m w.e., respectively) and close to the mass balance calculated from the glaciological method
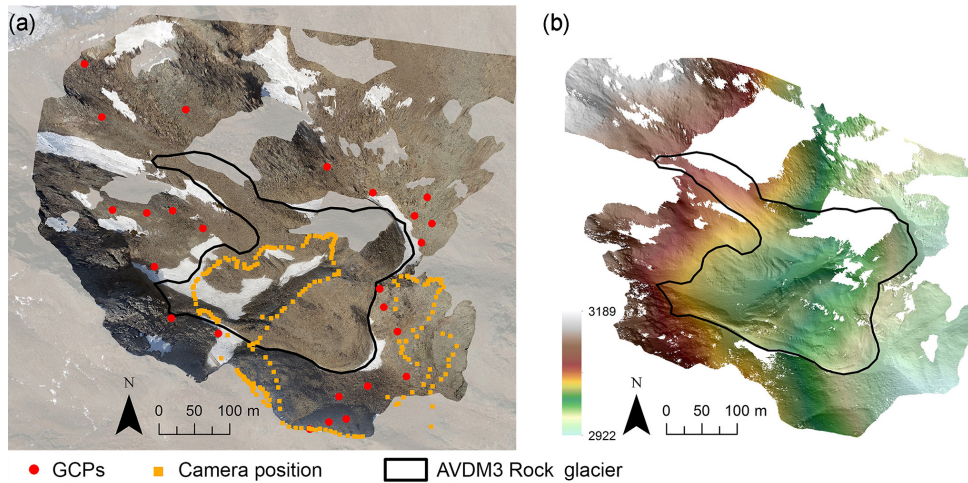
Figure 13. Correspondence between **(a)** the orthophoto of SfM–MVS 3-D model of rock glacier surveyed on 27 September 2014 and **(b)** the hillshade model overlain on colour-coded elevations of the rock glacier DEM calculated using the same data. The holes in the DEM are areas not reconstructed.
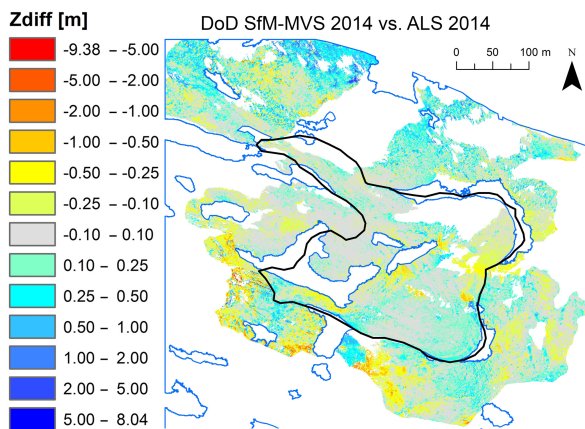
Figure 14. Spatial distribution of elevation differences between photogrammetric and ALS-based DEM acquired on 27 September and 24 September 2014, respectively. The blue outline is the snow accumulation areas which were excluded during the DEM comparison.

$(0.83 \pm 0.26\,\mathrm{m\,w.e.})$. The differences are well within the uncertainties of the glaciological and geodetic mass balance estimates, which were quantified following Zemp et al. (2013). These results confirm that the reliable mass balance estimates obtained by Piermattei et al. (2015) on the small Montasio Occidentale Glacier, in the Julian Alps, can also be replicated on larger glaciers with different morphologies and characteristics. The error of the geodetic estimates has been calculated in bare-ground areas outside the glacier, where the slope is lower than the 95° percentile of the slope frequency distribution inside the glacier (i.e. 40°) and under the conservative hypothesis that the standard error of the elevation differences among the DEMs is entirely correlated in space. This hy-

pothesis was adopted because there was no sufficiently large bare-ground area, with available DoD data, for analysing the scale of the spatial autocorrelation of elevation differences (e.g. Rolstad et al., 2009). As can be seen in Table 3, the significant uncertainty of the photogrammetric method can be mostly attributed to the 2013 survey, whereas the improvements of the 2014 survey led to a substantial reduction in the error.

Because the AVDM3 Rock glacier exhibits quite slow annual deformation and creep, we were able to calculate reliable displacement rates and area-averaged surface elevation changes on a multi-year (in our case, decadal) timescale. This result confirms the findings of Gómez-Gutiérrez et al. (2014), who applied a similar method to the Corral del Veleta Rock glacier in the Sierra Nevada (Spain), observing that this technique is suitable for medium-term (from 5- to 10-year intervals) monitoring of rock glacier surface displacements.

Our results are promising, despite the limitations of the adopted method, which include (i) the location of GCPs on natural targets outside the investigated glacier or rock glacier, (ii) the presence of areas with deep shadows and changes in light during the survey, (iii) the presence of fresh snow in the upper and middle part of the glacier, and (iv) the high camera–object distance in the glacier application.

In general terms, the photo-based accuracy is related to the image feature extraction, feature matching (in both the SfM and MVS steps) and scale definition (Bemis et al., 2014). A low accuracy in these steps, caused for example by poor camera network geometry, can generate model distortion and reduce the ability to identify unique corresponding features in overlapping images (Wackrow and Chandler, 2011; Dall'Asta et al., 2015; Favalli et al., 2012; James and Robson, 2012, 2014; Hosseininaveh et al., 2014; Micheletti et al., 2014; Nocerino et al., 2014). In our case studies, among the
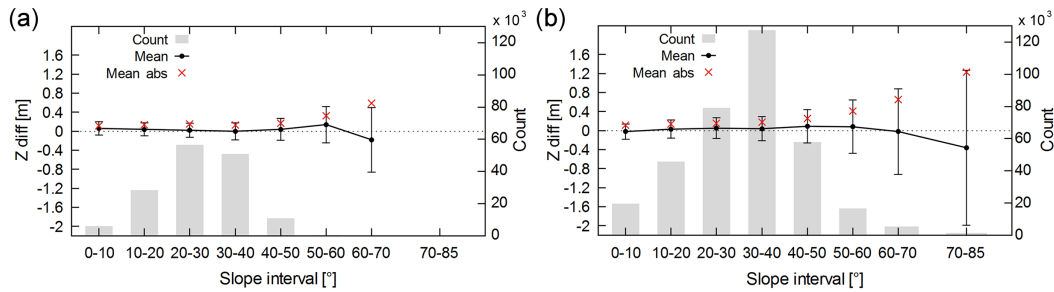
Figure 15. Mean, mean of the absolute values and standard deviation of elevation differences between 2014 SfM–MVS and ALS-based DEMs calculated for 10° intervals of slope **(a)** within the reconstructed area of the rock glacier and **(b)** on the bare ground outside the rock glacier.
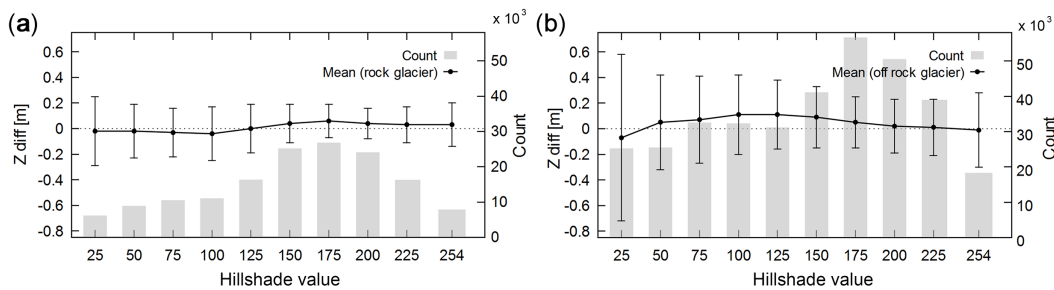
Figure 16. Elevation differences between 2014 SfM–MVS and ALS-based DEMs calculated for hillshade value intervals of 25 **(a)** in the rock glacier reconstructed area and **(b)** in the bare ground outside the rock glacier. Lowest values represent shadowed area, whilst well-lit areas have the highest values.

various aspects analysed, the spatial variability in the accuracy of the photogrammetric DEMs is related to the camera–object distance, the presence of fresh snow with low contrast, the changing illumination during the survey and the occurrence of shadows. The increasing error with increasing terrain slope suggests the persistence of a small shift in the reconstructed DEMs. This shift, however, does not affect the areal estimates of mass balance and elevation change, given that the vast majority of the glacier and rock glacier areas feature small or moderate slope angles. For both the glacier and the rock glacier, the spatial coverage of the reconstructed areas was not complete, ranging between 72 and 85 %. In the glacier surveys, the problematic areas were those visible from a low number of camera positions and those covered by fresh snow and far from the viewpoints. In the rock glacier, certain areas were not reconstructed due to the rock glacier's complex morphology and in particular to the presence of ridges, furrows and counterslopes.

5.2 Possible improvements of the SfM–MVS approach

The accuracy assessments confirm that the ALS data still provide results with somewhat higher accuracies (Tables 3 and 5, Figs. 6 and 14) but with much higher costs and demanding logistics than the SfM–MVS approach. However, the SfM–MVS method has the potential to provide a sig-

nificantly higher spatial resolution (Debella-Gilo and Kääb, 2011; Piermattei et al., 2015) and temporal resolution due to its significantly lower costs. Moreover, the photogrammetric reconstructions still have room for improvement, as demonstrated by the better results achieved from the 2014 survey of the glacier area compared to those from 2013. This improvement resulted from a higher number of photographs and improved camera network geometry.

Many of the limitations described above can be overcome by introducing modifications to the terrestrial photogrammetric survey strategy. For the rock glacier survey, shorter baselines are recommended to ensure greater spatial coverage, high image similarity and good matching performance (Wenzel et al., 2013). GCPs, for example, could be placed on the surface of the glaciers and rock glaciers to reduce the model distortions (Bemis et al., 2014) and generate surveys with much higher accuracies via, for example, the use of dGPS (differential GPS) to calculate their position (Dall'Asta et al., 2015).

The use of UAVs could solve the problem of excessive camera–object distances and the issue of missing areas due to inaccessibility. However, these alternatives imply increased costs, more troublesome logistics, greater expertise and ultimately longer survey times. In addition, they also require directly accessing unsafe or difficult to reach areas, both to place targets and to move UAVs among study areas that ex-
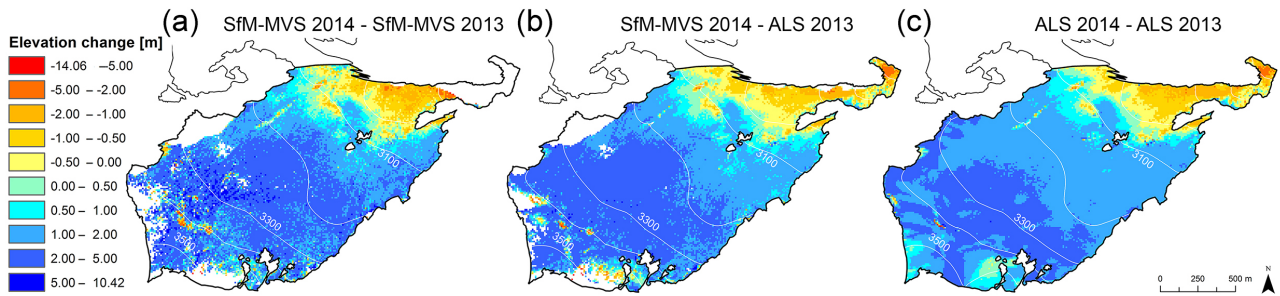
Figure 17. Spatial distribution of elevation changes between **(a)** SfM–MVS 2014 and SfM–MVS 2013 DEMs, **(b)** SfM–MVS 2014 and ALS 2013 over the area of the glacier with common coverage, and **(c)** ALS 2014 and ALS 2013 over the entire glacier.
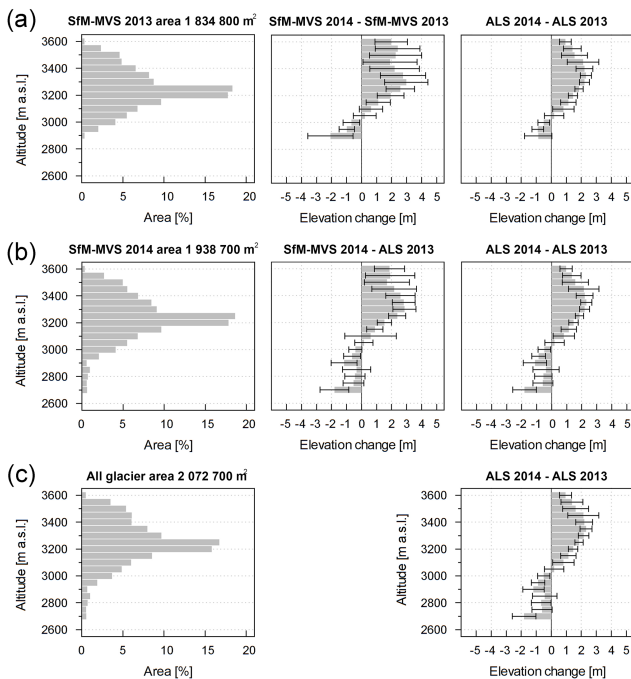
Figure 18. Area–altitude distribution and surface elevation change with standard deviation for the glaciological year 2014/2013 displayed for altitudinal bands with 50 m interval. The elevation changes were calculated between **(a)** SfM–MVS DEMs of 2013 and 2014 in the 2013 photogrammetric reconstructed area; **(b)** SfM–MVS DEMs of 2014 and ALS DEM of 2014 in the 2014 photogrammetric reconstructed area; **(c)** ALS DEMs of 2013 and 2014 of the entire glacier. The photogrammetric results were compared with the corresponding ALS results calculated in the same area.

ceed their operational range (Bühler et al., 2015). Therefore, the best balance must be found between simplicity, safety, costs and accuracy for each photogrammetric application based on the final objectives and on the available human and economic resources.

6 Conclusions

In this paper, we investigated the applicability of the SfM–MVS approach for monitoring glacial and periglacial processes in a catchment of the Ortles–Cevedale Group (eastern Italian Alps), validating our results using ALS DEMs as benchmarks. The ground surveys were conducted on foot and were intentionally planned to be as quick and easy as possible. The 2.1 km^2 La Mare Glacier and the neighbouring AVDM3 Rock glacier were surveyed in 1 day using only a consumer-grade SLR camera without the set-up of artificial targets.

The accuracy of the photogrammetric DEMs, evaluated as the mean and standard deviation of the elevation difference in a stable area between the SfM–MVS DEM and the reference ALS DEM, was $-0.42\,\mathrm{m} \pm 1.72\,\mathrm{m}$ and $0.03\,\mathrm{m} \pm 0.74\,\mathrm{m}$ for the 2013 and 2014 surveys, respectively. The SfM–MVS DEM accuracy of the reconstructed rock glacier surface acquired in 2014 was estimated to be $0.02\,\mathrm{m} \pm 0.17\,\mathrm{m}$.

The SfM–MVS geodetic mass balance estimates for the La Mare Glacier were in good agreement with the calculations from the contemporary ALS data and with the results of the glaciological method, confirming a positive mass balance of approximately 0.9 m w.e. in the 2013–14 hydrological year. In the rock glacier, the survey produced a good spatial coverage of the photogrammetric DEM and a reliable calculation of the multi-year surface changes ($-0.18\,\mathrm{m}$ on overage) and displacement rates ($0.18\,\mathrm{m\,yr^{-1}}$ on average) in the period from 2003 to 2014. For rock glacier applications, particularly for slow-mowing ones such as AVDM3, single-year assessments of elevation change and surface velocities require the set-up of artificial targets and GCPs to obtain the accuracy required to detect such slow processes.

The simplicity of the ground surveys and the physical characteristics of the analysed alpine terrain were the main factors influencing the approach tested. In particular, we refer to the use of natural targets as GCPs, the occurrence of shadowed areas and lighting changes during the surveys, the presence of fresh snow in the upper part of the glacier (which reduced the contrast), and the suboptimal camera network
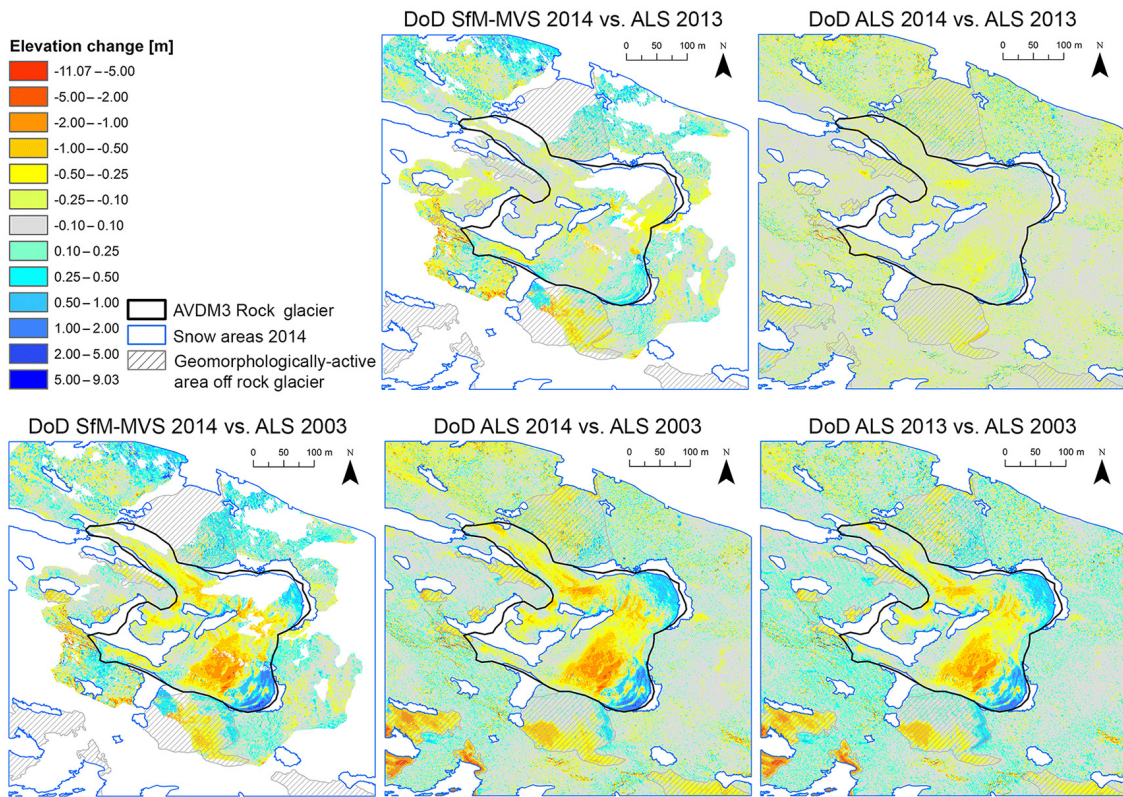
Figure 19. Spatial distribution of elevation changes from September 2014 to September 2013 and from September 2003 between the DEMs derived from SfM–MVS and ALS.
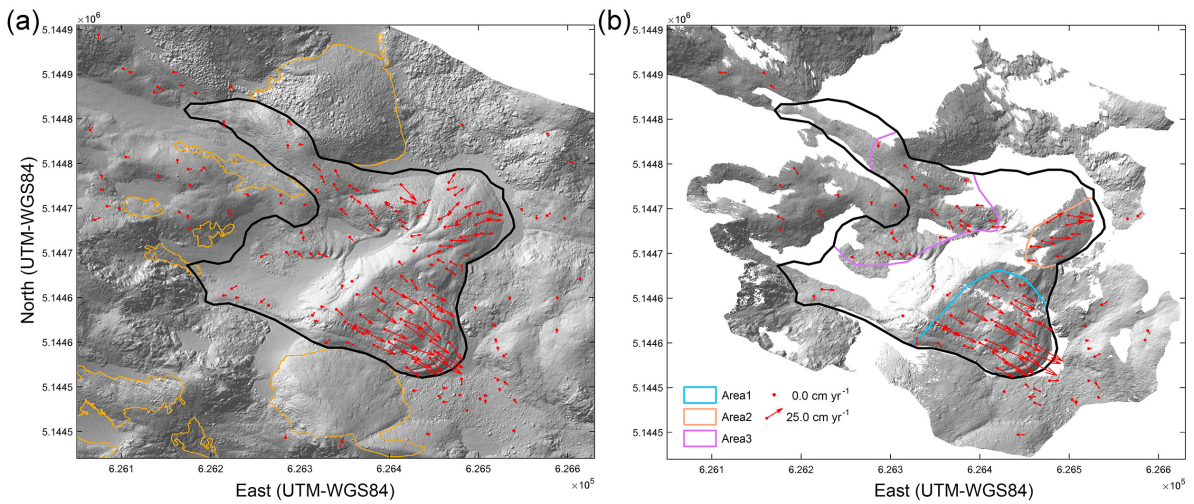
Figure 20. Displacement vectors of the rock glacier between 2003 and 2014 computed by a manual identification of natural features visible in the hillshaded DEMs generated by **(a)** ALS for both survey epochs and by **(b)** ALS and photogrammetry for 2003 and 2014 survey, respectively.

geometry and long camera–object distances imposed by the morphology and accessibility of the study area. Consideration the factors that spatially control the accuracy of the SfM–MVS DEMs, there remains room for significant improvements, e.g. using aerial platform and/or placing artificial targets surveyed by dGPS. Further research is therefore needed to (i) find technical solutions to overcome the major limitations of the SfM–MVS approach in such remote areas and (ii) achieve the optimal balance between the simplicity and low cost of this approach and the accuracy required for each specific application.

Data availability

The data set acquired and processed in this work is made available upon request to the first author of the manuscript. For the other data sets mentioned in this work, please contact the Cryosphere AND Hydrology group of the University of Padova, http://intra.tesaf.unipd.it/CMS/glaciology/default.asp.

References

AgiSoft LLC: AgiSoft PhotoScan Professional Edition. Version 1.1.2, available at: http://www.agisoft.ru/products/photoscan/ (last access: 18 January 2015), 2010a.

AgiSoft LLC: AgiSoft PhotoScan User-manuals Version 1.0, available at: http://www.agisoft.com/pdf/photoscan-pro_1_1_en.pdf (last access: 15 May 2015), 2010b.

Astronomical Applications – U.S. Naval Observatory, Sun or Moon Altitude/Azimuth Table, available at: http://aa.usno.navy.mil/data/docs/AltAz.php, last access: 1 April 2015.

Bemis, S., Micklethwaite, S., and Turner, D.: Ground-based and UAV-Based photogrammetry: a multi-scale, high-resolution mapping tool for Structural Geology and Paleoseismology, J. Struct. Geol., 69, 163–178, doi:10.1016/j.jsg.2014.10.007, 2014.

Bertone, A.: Misure di spostamento dei rock glacier con l'uso di feature tracking applicato a DTM multitemporali, BSc Thesis, Department of Earth and Environmental Sciences, University of Pavia, Pavia, Italy, 63 pp., 2014.

Besl, P. J. and McKay, N. D.: Method for registration of 3-D shapes, in: Proceedings of the International Society for Optics and Photonics IEEE Transactions on Pattern Analysis and Machine Intelligence, 1611, 586–606, 1992.

Bradley, D., Boubekeur, T., and Heidrich, W.: Accurate multiview reconstruction using robust binocular stereo and surface meshing, in: IEEE Conference on Computer Vision and Pattern Recognition, Anchorage, AK, USA, 1–8, 2008.

Bühler, Y., Marty, M., Egli, L., Veitinger, J., Jonas, T., Thee, P., and Ginzler, C.: Snow depth mapping in high-alpine catchments using digital photogrammetry, The Cryosphere, 9, 229–243, doi:10.5194/tc-9-229-2015, 2015.

Carturan, L.: Climate change effects on the cryosphere and hydrology of a high-altitude watershed, PhD thesis, Department of Land, Environment, Agriculture and Forestry, University of Padova, Padova, Italy, 2010.

Carturan, L.: Replacing monitored glaciers undergoing extinction: a new measurement series on La Mare Glacier (Ortles-Cevedale, Italy), J. Glaciol., in review, 2016.

Carturan, L., Baroni, C., Carton, A., Cazorzi, F., Fontana, G. D., Delpero, C., and Zanoner, T.: Reconstructing Fluctuations of La Mare Glacier (Eastern Italian Alps) in the Late Holocene: new Evidence for a Little Ice Age Maximum Around 1600 AD. Geografiska Annaler: Series A, Physical Geography, 96, 287–306, 2014.

Carturan, L., Zuecco, G., Seppi, R., Zanoner, Z., Borga, M., Carton, A., and Dalla Fontana, G.: Catchment-scale permafrost mapping using spring water characteristics, Permafrost Periglac., doi:10.1002/ppp.1875, 2015.

Chen, Y. and Medioni, G.: Object modeling by registration of multiple range images, in: Proceedings, IEEE International Conference on Robotics and Automation, 9–11 April, Sacramento, CA, USA, 10, 145–155, 1991.

Cryosphere and Hydrology group: Research group of the University of Padova, available at: http://intra.tesaf.unipd.it/CMS/glaciology/default.asp, last access: 19 May 2016.

Dall'Asta, E., Delaloye, R., Diotri, F., Forlani, G., Fornari, M., Morra di Cella, U., Pogliotti, P., Roncella, R., and Santise, M.: Use of UAS in a high mountain landscape: the case of gran sommetta rock glacier (AO), The International Archives of the Photogrammetry, Remote Sensing and Spatial Information Sciences, Volume XL-3/W3, 391–397, 2015.

Debella-Gilo, M. and Kääb, A.: Sub-pixel precision image matching for measuring surface displacements on mass movements using normalized cross-correlation, Remote Sens. Environ., 115, 130–142, 2011.

Favalli, M., Fornaciai, A., Isola, I., Tarquini, S., and Nannipieri, L.: Multiview 3-D reconstruction in geosciences, Comput. Geosci., 44, 168–176, 2012.

Gauthier, D., Conlan, M., and Jamieson, B.: Photogrammetry of fracture lines and avalanche terrain: potential applications to research and hazard mitigation projects, Proceedings, International Snow Science Workshop, Banff, 29 September–3 October 2014, 109–115, 2014.

Glira, P., Pfeifer, N., Briese, C., and Ressl, C.: A correspondence framework for ALS strip adjustments based on variants of the ICP algorithm, Photogramm. Fernerkun., 4, 275–289, doi:10.1127/pfg/2015/0270, 2015.

Gómez-Gutiérrez, Á., de Sanjosé-Blasco, J. J., de Matías-Bejarano, J., and Berenguer-Sempere, F.: Comparing two photoreconstruction methods to produce high density point clouds and DEMs in the Corral del Veleta Rock Glacier (Sierra Nevada, Spain), Remote Sensing, 6, 5407–5427, 2014.

Gómez-Gutiérrez, Á., de Sanjosé-Blasco, J. J., Lozano-Parra, J., Berenguer-Sempere, F., and de Matías-Bejarano, J.: Does HDR pre-processing improve the accuracy of 3-D models obtained by means of two conventional SfM-MVS software packages? The case of the Corral del Veleta Rock Glacier, Remote Sensing, 7, 10269–10294, 2015.

Hartley, R. and Zisserman, A.: Multiple View Geometry, In Computer Vision, Cambridge University Press, Cambridge, UK, 2003.

Haeberli, W.: Creep of mountain permafrost: internal structure and flow of alpine rock glaciers, Mitteilungen der Versuchsanstalt für Wasserbau, Hydrologie und Glaziologie der ETH Zurich, 77, 5–142, 1985.

Hosseininaveh, A., Sargeant, B., Erfani, T., Robson, S., Shortis, M., Hess, M., and Boehm, J.: Towards fully automatic reliable 3-D acquisition: from designing imaging network to a complete and accurate point cloud, Robotics and Autonomous Systems, 62, 1197–1207, 2014.

Huss, M.: Density assumptions for converting geodetic glacier volume change to mass change, The Cryosphere, 7, 877–887, doi:10.5194/tc-7-877-2013, 2013.

Immerzeel, W. W., Kraaijenbrink, P. D. A., Shea, J. M., Shrestha, A. B., Pellicciotti, F., Bierkens, M. F. P., and De Jong, S. M.: High-resolution monitoring of Himalayan glacier dynamics using unmanned aerial vehicles, Remote Sens. Environ., 150, 93–103, 2014.

Isaksen, K., Ødegård, R. S., Eiken, T., and Sollid, J. L.: Composition, flow and development of two tongue-shaped rock glaciers in the permafrost of Svalbard. Permafrost and Periglacial Processes, 11, 241–257, 2000.

James, M. R. and Robson, S.: Straightforward reconstruction of 3-D surfaces and topography with a camera: accuracy and geoscience application, J. Geophys. Res.-Earth, 117, F03017, doi:10.1029/2011JF002289, 2012.

James, M. R. and Robson, S.: Mitigating systematic error in topographic models derived from UAV and ground-based image networks, Earth Surf. Proc. Land. 39, 1413–1420, doi:10.1002/esp.3609, 2014.

Kääb, A.: Monitoring high-mountain terrain deformation from repeated air-and spaceborne optical data: examples using digital aerial imagery and ASTER data, ISPRS J. Photogramm., 57, 39–52, 2002.

Kääb, A.: Remote Sensing of Mountain Glaciers and Permafrost Creep. Research Perspectives from Earth Observation Technologies and Geoinformatics, Schriftenreihe Physische Geographie, Glaziologie und Geomorphodynamik, 48, University of Zurich, Zurich, Switzerland, 2005.

Kääb, A., Kaufmann, V., Ladstädter, R., and Eiken, T.: Rock glacier dynamics: implications from high-resolution measurements of surface velocity fields, in: Eighth International Conference on Permafrost, 21–25 July 2003, Zurich, Switzerland, 1, 501–506, 2003.

Kääb, A., Girod, L., and Berthling, I.: Surface kinematics of periglacial sorted circles using structure-from-motion technology, The Cryosphere, 8, 1041–1056, doi:10.5194/tc-8-1041-2014, 2014.

Micheletti, N., Chandler, J. H., and Lane, S. N.: Investigating the geomorphological potential of freely available and accessible Structure-from-Motion photogrammetry using a smartphone,

Earth Surf. Proc. Land., 40, 473–486, doi:10.1002/esp.3648, 2014.

Nilosek, D., Sun, S., and Salvaggio, C.: Geo-accurate model extraction from three-dimensional image-derived point clouds, in: Proceedings of SPIE, Algorithms and Technologies for Multispectral, Hyperspectral, and Ultraspectral Imagery XVIII, 23 April 2012, Baltimore, MD, USA, 8390, 83900J, doi:10.1117/12.919148, 2012.

Nocerino, E., Menna, F., and Remondino, F.: Accuracy of typical photogrammetric networks in cultural heritage 3-D modeling projects, ISPRS-International Archives of the Photogrammetry, Remote Sensing and Spatial Information Sciences, 1, 465–472, 2014.

Østrem, G. and Brugman, M.: Glacier mass-balance measurements: A manual for field and office work, NHRI Science Report, Saskatoon, Canada, 224 pp., 1991.

Piermattei, L., Carturan, L., and Guarnieri, A.: Use of terrestrial photogrammetry based on structure from motion for mass balance estimation of a small glacier in the Italian Alps, Earth Surf. Proc. Land., 40, 1791–1802, doi:10.1002/esp.3756, 2015.

Ryan, J. C., Hubbard, A. L., Box, J. E., Todd, J., Christoffersen, P., Carr, J. R., Holt, T. O., and Snooke, N.: UAV photogrammetry and structure from motion to assess calving dynamics at Store Glacier, a large outlet draining the Greenland ice sheet, The Cryosphere, 9, 1–11, doi:10.5194/tc-9-1-2015, 2015.

Roer, I. and Nyenhuis, M.: Rockglacier activity studies on a regional scale: comparison of geomorphological mapping and photogrammetric monitoring, Earth Surf. Proc. Land., 32, 1747–1758, 2007.

Rolstad, C., Haug, T., and Denby, B.: Spatially integrated geodetic glacier mass balance and its uncertainty based on geostatistical analysis: Application to the western Svartisen ice cap, Norway. J. Glaciol., 55, 666–680, doi:10.3189/002214309789470950, 2009.

Seppi, R., Carton, A., Zumiani, M., Dall'Amico, M., Zampedri, G., and Rigon, R.: Inventory, distribution and topographic features of rock glaciers in the southern region of the Eastern Italian Alps (Trentino), Geografia Fisica e Dinamica Quaternaria, 35, 185–197, doi:10.4461/GFDQ.2012.35.17, 2012.

Solbø, S. and Storvold, R.: Mapping svalbard glaciers with the cryowing uas, ISPRS International Archives of the Photogrammetry, Remote Sensing and Spatial Information Sciences, XL-1/W2, 373–377, 2013.

Tonkin, T. N., Midgley, N. G., Graham, D. J., and Labadz, J. C.: The potential of small unmanned aircraft systems and structure-from-motion for topographic surveys: a test of emerging integrated approaches at Cwm Idwal, North Wales, Geomorphology, 226, 35–43, 2014.

Triggs, B., McLauchlan, P. F., Hartley, R. I., and Fitzgibbon, A. W.: Bundle adjustment – A modern synthesis, in: Vision algorithms: theory and practice, Springer Berlin Heidelberg, 298–372, 1999.

Tseng, C.-M., Lin, C. W., Dalla Fontana, G., and Tarolli, P.: The topographic signature of a Major Typhoon, Earth Surf. Proc. Land., 40, 1129–1136, 2015.

Verhoeven, G., Karel, W., Stuhec, S., Doneus, M., Trinks, I., and Pfeifer, N.: Mind your grey tones – examining the influence of decolourization methods on interest point extraction and matching for architectural image-based modelling, in: 3-D-Arch 2015–3-D Virtual Reconstruction and Visualization of Complex Archi-

tectures (ISPRS WG V/4, CIPA), 25–27 February 2015, 40, IS-PRS, Avila, Spain, 307–314, 2015.

Zemp, M., Thibert, E., Huss, M., Stumm, D., Rolstad Denby, C., Nuth, C., Nussbaumer, S. U., Moholdt, G., Mercer, A., Mayer, C., Joerg, P. C., Jansson, P., Hynek, B., Fischer, A., Escher-Vetter, H., Elvehøy, H., and Andreassen, L. M.: Reanalysing glacier mass balance measurement series, The Cryosphere, 7, 1227–1245, doi:10.5194/tc-7-1227-2013, 2013.

Wackrow, R. and Chandler, J.: Minimising systematic error surfaces in digital elevation models using oblique convergent imagery, Photogramm. Rec., 26, 16–31, 2011.

Wenzel, K., Rothermel, M., Fritsch, D., and Haala, N.: Image acquisition and model selection for multi-view stereo, Int. Arch. Photogramm. Remote Sens. Spatial Inf. Sci, 251–258, 2013.

Whitehead, K., Moorman, B. J., and Hugenholtz, C. H.: Brief Communication: Low-cost, on-demand aerial photogrammetry for glaciological measurement, The Cryosphere, 7, 1879–1884, doi:10.5194/tc-7-1879-2013, 2013.

Zemp, M., Thibert, E., Huss, M., Stumm, D., Rolstad Denby, C., Nuth, C., Nussbaumer, S. U., Moholdt, G., Mercer, A., Mayer, C., Joerg, P. C., Jansson, P., Hynek, B., Fischer, A., Escher-Vetter, H., Elvehøy, H., and Andreassen, L. M.: Reanalysing glacier mass balance measurement series, The Cryosphere, 7, 1227–1245, doi:10.5194/tc-7-1227-2013, 2013.